Nanoscale

PAPER

View Article Online
View Journal | View Issue

Cite this: *Nanoscale*, 2016, **8**, 11924

Analysing intracellular deformation of polymer capsules using structured illumination microscopy†

Xi Chen, Jiwei Cui, Huanli Sun,‡ Markus Müllner,§ Yan Yan,¶ Ka Fung Noi, Yuan Ping‖ and Frank Caruso*

Received 15th March 2016,
Accepted 16th May 2016

DOI: 10.1039/c6nr02151d

www.rsc.org/nanoscale

Understanding the behaviour of therapeutic carriers is important in elucidating their mechanism of action and how they are processed inside cells. Herein we examine the intracellular deformation of layer-by-layer assembled polymer capsules using super-resolution structured illumination microscopy (SIM). Spherical- and cylindrical-shaped capsules were studied in three different cell lines, namely HeLa (human epithelial cell line), RAW264.7 (mouse macrophage cell line) and differentiated THP-1 (human monocyte-derived macrophage cell line). We observed that the deformation of capsules was dependent on cell line, but independent of capsule shape. This suggests that the mechanical forces, which induce capsule deformation during cell uptake, vary between cell lines, indicating that the capsules are exposed to higher mechanical forces in HeLa cells, followed by RAW264.7 and then differentiated THP-1 cells. Our study demonstrates the use of super-resolution SIM in analysing intracellular capsule deformation, offering important insights into the cellular processing of drug carriers in cells and providing fundamental knowledge of intracellular mechanobiology. Furthermore, this study may aid in the design of novel drug carriers that are sensitive to deformation for enhanced drug release properties.

1 Introduction

Over the past two decades, polymer capsules have evolved from hollow polyelectrolyte constructs to promising tailor-made nanoreactors and drug delivery systems.[1,2] In particular, nanoengineered polymer capsules fabricated through layer-by-layer (LbL) assembly are promising candidates for the intracellular delivery of therapeutics due to the control that can be exerted over their surface chemistry, size, shape, and cargo loading/release.[3,4] Given their versatile properties, such polymer capsules have been engineered to be readily internalised by a wide range of cell lines, including epithelial cells and various immune cells.[5] The potential application of LbL capsules in drug delivery and other biological applications highlights the importance of elucidating a fundamental understanding of their interaction with biological systems.[5,6] To this end, the intracellular processing and intracellular fate of the capsules are important aspects.[7]

The deformation of polymer capsules upon the internalisation process provides insight into their stability and the potential mechanism of action inside the cells.[8–11] Confocal laser scanning microscopy (CLSM) revealed that 5 μm polymer capsules are internalised by human breast cancer cells (MDA-MB-435s), but the shape of the internalised capsules differs significantly from those remaining outside the cells.[8] The change in shape is believed to be caused by force-driven deformation within the endocytic compartments in which the capsules are trapped. A study on the deformation of polymer capsules of 2.0 to 3.5 μm diameter upon intracellular uptake by HeLa cells, investigated by atomic force microscopy (AFM), suggested that the tracking of polymer capsules can be used to examine the mechanical properties of living cells through their uptake process.[12] These results revealed that the polymer capsules deformed upon internalisation, and that this was caused by a mechanical deformation process that exhibits intracellular forces that the polymer capsules cannot withstand

ARC Centre of Excellence in Convergent Bio-Nano Science and Technology, and the Department of Chemical and Biomolecular Engineering, The University of Melbourne, Parkville, Victoria 3010, Australia. E-mail: fcaruso@unimelb.edu.au

† Electronic supplementary information (ESI) available: Additional figures. See DOI: 10.1039/c6nr02151d

‡ Present address: Biomedical Polymers Laboratory, and Jiangsu Key Laboratory of Advanced Functional Polymer Design and Application, College of Chemistry, Chemical Engineering and Materials Science, Soochow University, Suzhou, 215123, China.

§ Present address: Key Centre for Polymers and Colloids, School of Chemistry, University of Sydney, Sydney, NSW 2006, Australia.

¶ Present address: Centre for BioNano Interactions, School of Chemistry and Chemical Biology, University College Dublin, Belfield, Dublin 4, Ireland.

‖ Present address: School of Materials Science and Engineering, Nanyang Technological University, Singapore 639798, Singapore.

during internalisation.[13] This is in agreement with our previous transmission electron microscopy (TEM) study where polymer capsules (850 nm) appeared distorted in the late endosomes or lysosomes of a human colon cancer derived cell line (LIM 1899).[14] These deformation-based studies indicate that the intracellular processes can vary dramatically for different polymer capsules due to differences in their physicochemical properties, as well as cell physiology.[15,16] Therefore, in this work, we investigate the intracellular deformation of polymer capsules of size more applicable for intracellular drug delivery, and examine the effect of shape and cell line on capsule deformation.

Most cellular events are highly dynamic, therefore, tracking them under biological conditions requires high temporal resolution of the analytical procedure employed.[17] Live cell imaging may be used; however, determining subtle changes in the morphology of nanostructures upon interaction with biological systems is often challenging using conventional microscopy, such as confocal or deconvolution microscopy. We have previously reported the deformation of spherical polymer capsules (diameter (D) = 390–850 nm) in different cell lines, including human cervical cancer cell line HeLa (HeLa), mouse leukemia cell line RAW264.7 (RAW), and differentiated human leukemia cell line THP-1 (dTHP-1).[18–20] However, given the resolution limits of conventional microscopy, any differences in the intracellular deformation of polymer capsules were not able to be resolved. Recently, stochastic optical reconstruction microscopy (STORM) and structured illumination microscopy (SIM) techniques have been applied for imaging the internalisation and intracellular processing of nanoparticles.[21–23]

Herein we examine the intracellular deformation of polymer capsules in different cell lines using the super high resolution microscopy technique, SIM. SIM provides more than a two-fold increase in resolution by collecting information from the frequency space outside the observable region, and is able to clearly identify nanostructures (*ca.* 110 nm in X/Y resolution) compared with other conventional microscopes (*ca.* 250 nm in X/Y resolution).[17,23–25] Thiolated poly(methacrylic acid) (PMA_{SH}) capsules with two different shapes (spherical: D = 390 nm and cylindrical: 2020 × 310 nm) were prepared *via* LbL assembly. The cellular association of these PMA_{SH} capsules with three different cell lines (HeLa, RAW and dTHP-1) was subsequently investigated. Negligible differences in the cellular association with spherical capsules were observed between HeLa, RAW and dTHP-1 cells; however, significant differences in the cellular association with cylindrical capsules were observed with each cell line. Subsequently, the intracellular deformation of polymer capsules was tracked using SIM and our results show that hollow structured PMA_{SH} capsules, whether spherical and cylindrical in shape, exhibit different levels of deformation depending on the cell line. PMA_{SH} capsules morphed from hollow spheres to more dense particles after being internalised by HeLa cells. In contrast, PMA_{SH} capsules largely retained their original morphology after uptake by dTHP-1 cells. With the use of SIM, our findings provide a better insight into the deformation of the polymer capsules inside cells. This information may aid in the development of rationally designed polymer capsules and opens up new possibilities in the design and investigation of particle–cell interactions.

2 Experimental section

2.1 Materials

Silica (SiO_2) particles (D = 235 nm) were purchased from Micro-Particles (GmbH, Germany). 1-(3-Dimethylaminopropyl)-3-ethylcarbodiimide (EDC), tetraethyl orthosilicate (TEOS), sodium acetate (NaOAc), phosphate-buffered saline (PBS), *N*-chloro-*p*-toluenesulfonamide sodium salt (chloramine-T hydrate), hydrofluoric acid (HF), poly(*N*-vinylpyrrolidone) (PVPON, M_w 10 and 40 kDa), 4-(4,6-dimethoxy-1,3,5-triazin-2-yl)-4-methylmorpholinium chloride (DMTMM), dithiothreitol (DTT), 3-(*N*-morpholino)propanesulfonic acid (MOPS), 2-(*N*-morpholino)ethanesulfonic acid (MES), and 12-*O*-tetradecanoylphorbol-13-acetate (TPA) were purchased from Sigma-Aldrich and used as received. Poly(methacrylic acid) sodium salt (PMA, M_w 15 kDa, 30 wt% in water) was obtained from Polysciences (USA). Pyridine dithioethylamine hydrochloride (PDA-HCl) was purchased from Shanghai Speed Chemical Co. Ltd, China. Alexa Fluor 633 (AF633) hydrazide and AF488 goat antimouse IgG were acquired from Invitrogen. Roswell Park Memorial Institute (RPMI) medium, Dulbecco's Modified Eagle Medium (DMEM), fetal bovine serum (FBS), 4% paraformaldehyde (PFA), Dulbecco's phosphate-buffered saline (DPBS), AF488 phalloidin, AF488 wheat germ agglutinin (WGA) and SnakeSkin™ dialysis tubing (3.5 kDa molecular weight cut-off) were purchased from Thermo Fisher Scientific Australia Pty Ltd. Mouse anti-human LAMP-1 antibody (CD107a) was obtained from BD Pharmingen (USA). For all experiments, high-purity water with a resistivity greater than 18.0 MΩ cm (Milli-Q water) was obtained from an in-line Millipore RiOs/Synergy purification system.

2.2 Synthesis of PMA_{SH}

Poly(methacrylic acid) with 12% thiol group modification was synthesised as reported elsewhere.[26] Briefly, a PMA solution (187.15 mg) was diluted with 3 mL of phosphate buffer (50 mM, pH 7.4). The resulting solution was activated with 43 mg of EDC and the mixture was stirred at ambient temperature for 30 min. Subsequently, 28.36 mg of PDA-HCl was added to the mixture and the reaction was allowed to proceed for 24 h. The resulting solution was purified *via* dialysis for 3 days against Milli-Q water and subsequently freeze dried for 48 h to obtain PMA–PDA as a powder. The degree of PDA modification of PMA was quantified using a NanoDrop 1000 spectrophotometer (Thermo Scientific). To expose thiol groups, PMA–PDA was incubated with 0.5 M DTT solution in MOPS buffer (20 mM, pH 8) to a concentration of 100 g L^{-1} mixed for 20 min at 37 °C with shaking. The stock solution was then diluted with NaOAc buffer (50 mM, pH 4) to the desired concentration prior to LbL assembly.

2.3 Synthesis of SiO_2 particles with cylindrical shapes

SiO_2 particles with cylindrical shapes were fabricated according to the method reported by Kuijk *et al.*[27] Briefly, 3 g of PVPON (M_w 40 kDa) was dissolved in 30 mL of 1-pentanol by sonication for 4 h. Then, 0.8 mL of Milli-Q water, 0.2 mL of sodium citrate dihydrate solution (0.18 M in water), 3 mL of ethanol, and 0.7 mL of ammonia (28 wt%) were separately added to the mixture. The solution was mixed by hand for 1 min and then kept static for 5 min, followed by the addition of 0.3 mL of TEOS (99%). After gentle shaking by hand for 1 min, the bottle was kept static to allow the reaction to proceed at 37 °C for 60 min to obtain the cylindrical SiO_2 particles. To purify the as-synthesised rods, the middle layer of the reaction mixture was collected and centrifuged at 3000*g* for 30 min. The pellet was washed twice with ethanol, then twice with Milli-Q water and finally suspended in Milli-Q water. The SiO_2 particles with cylindrical shape obtained were characterised using TEM, as shown in Fig. S1.†

2.4 Assembly of PMA_{SH} capsules

The SiO_2 particles (5 mg) were washed three times with NaOAc buffer (50 mM, pH 4) by centrifugation for two min at 1000*g*. The particles were then suspended in 50 μL NaOAc buffer by vortexing and sonication for 5 min. PVPON solution (50 μL, 4 g L^{-1} in 50 mM NaOAc buffer) was then added to the SiO_2 particles and incubated with mixing for 10 min to allow polymer adsorption. After incubation, the PVPON-coated particles were washed three times with NaOAc buffer and then suspended in 50 μL NaOAc buffer. PMA_{SH} solution (50 μL, 4 g L^{-1} in 50 mM NaOAc buffer) was then added and incubated for 10 min. The particles were washed three times with NaOAc buffer and finally suspended in 50 μL NaOAc buffer. The adsorption of PVPON and then PMA_{SH} constituted the assembly of a single bilayer. The layering process was repeated until four bilayers were deposited with PVPON as the outermost layer. The polymer multilayers were crosslinked by disulfide bridging through oxidation of the thiol groups of PMA_{SH}. In brief, PVPON/PMA_{SH} core–shell particles were incubated in MES buffer (50 mM, pH 6) with gentle shaking overnight in the presence of 2.8 mM chloramine-T (reversible crosslinking) or (1,8-bismaleimido)diethyleneglycol ($BM(PEG)_2$, irreversible crosslinking). The crosslinked core–shell particles were collected by washing twice with MES buffer and then twice with NaOAc buffer. The capsules were obtained by dissolving the SiO_2 templates using 5 M HF for 5 min (*Caution!* HF is corrosive and highly toxic! Extreme care must be taken when handling!), followed by three washing and redispersion cycles with PBS buffer. The capsules were then fluorescently labelled by mixing them with 5 μL of AF633 hydrazide and 1 mg of DMTMM in 200 μL PBS for 12 h. The fluorescently labelled capsules were obtained *via* centrifugation and washing with PBS four times.

2.5 Characterisation of PMA_{SH} capsules

TEM (Philips CM120 BioTWIN, operated at 120 kV) was used to determine the capsule size and morphology (at least 100 capsules were imaged and analysed). The fluorescently labelled PMA_{SH} capsules were imaged with SIM (DeltaVision OMX Blaze 3D-SIM from Applied Precision). Film thicknesses of the PMA_{SH} capsules were measured by AFM using an MFP-3D atomic force microscope (Asylum Research). Imaging was performed using ultrasharp SiN gold-coated cantilevers (NT-MDT). Capsule counting was performed using an Apogee A50-Micro flow cytometer (Apogee Flow Systems Ltd) with a laser excitation wavelength of 638 nm.

2.6 Cell culture

HeLa and RAW cells were cultured in DMEM GlutaMAX supplemented with 10% FBS at 37 °C in a 5% CO_2-humidified atmosphere and subcultured prior to confluence using trypsin. dTHP-1 cells were differentiated from THP-1 cells by incubation with 200 nM TPA for 48 h in complete RPMI medium (RPMI contains 10% FBS, termed cRPMI) at 37 °C in a 5% CO_2-humidified atmosphere.

2.7 Cellular association

HeLa, RAW and dTHP-1 cells were plated in 12-well plates at a density of 1×10^5 cells per well and allowed to adhere overnight. The cells were then incubated with PMA_{SH} capsules at a capsule-to-cell ratio of 100 : 1 for a 24 h period at 37 °C in 5% CO_2. After incubation, the cells were gently washed three times with DPBS and then harvested by trypsinization at 37 °C. At least 10 000 cells were analysed by flow cytometry.

2.8 Intracellular deformation of PMA_{SH} capsules

HeLa, RAW and dTHP-1 cells were plated in 8-well Lab-Tek I chambered coverglass slides (Thermo Fisher Scientific, Rochester) at a density of 3×10^4 cells per well. The cells were then treated with PMA_{SH} capsules at a capsule-to-cell ratio of 100 : 1 for 24 h at 37 °C in 5% CO_2. After incubation, the cells were fixed with 4% PFA for 10 min at 25 °C and the membrane was stained by incubation with AF488 WGA (0.5 μg mL^{-1}) for 10 min at 25 °C, followed by washing with DPBS three times. For actin staining, the cells were fixed and then 500 μL of Triton X-100 (0.1% in PBS buffer) was used to permeabilise the cells for 5 min at 25 °C. Subsequently, the actin was stained by incubation with AF488 phalloidin (0.5 μg mL^{-1}) for 20 min at 25 °C. Fluorescence images and optical sections were collected using a SIM equipped with a 60 × 1.24 NA oil objective under a FITC/CY5 filter set. Images were processed with Imaris 6.3.1 (Bitplane).

2.9 Intracellular fate

HeLa, RAW or dTHP-1 cells (3×10^4) were plated per well in 8-well Lab-Tek I chambered coverglass slides, and incubated with PMA_{SH} capsules at a capsule-to-cell ratio of 100 : 1 at 37 °C in 5% CO_2. After 24 h incubation, the cells were fixed with 4% PFA for 10 min at 25 °C. To permeabilise the cells for immunostaining, the fixed cells were incubated with 500 μL Triton X-100 (0.1% in PBS buffer) for 5 min at 25 °C. Late endosomes and lysosomes were then immunostained with 200 μL of mouse anti-human antibody (LAMP1, 2.5 μg mL^{-1})

followed by 200 μL of AF488 goat anti-mouse IgG (2 μg mL^{-1}) for 45 min at 25 °C. Fluorescence images and optical sections were collected using a SIM equipped with a 60 × 1.24 NA oil objective under a FITC/CY5 filter set. Images were processed with Imaris 6.3.1 (Bitplane).

3 Results and discussion

3.1 Preparation and characterisation of PMA_{SH} capsules with spherical and cylindrical shapes

PMA_{SH} capsules were prepared according to the protocol reported previously.[18] Briefly, spherical and cylindrical SiO_2 templates were sequentially coated with PVPON/PMA_{SH} *via* hydrogen bonding-mediated LbL assembly, followed by the oxidative crosslinking of thiol groups on PMA_{SH} layers. Upon removal of the sacrificial SiO_2 templates and PVPON layers, homogeneous and well-dispersed PMA_{SH} capsules were obtained. The dimensions of the obtained PMA_{SH} capsules were examined by TEM, revealing spherical (390 × 390 nm, Fig. 1A) and cylindrical (2020 × 310 nm, Fig. 1D) capsules. The size increase of the capsules compared with the corresponding templates is due to swelling of the capsule wall after removal of the template support.[28] Both types of capsules retained their original morphology after template removal. AFM was used to determine the wall thickness of the PMA_{SH} capsules. The measured height profile was consistent across all capsules, indicating homogeneous LbL build-up (Fig. 1C and F), with an average thickness of 3.5 nm per polymer layer (Fig. S2†).

3.2 Cell association kinetics

The association, which encompasses binding and/or internalisation, of PMA_{SH} capsules with various cell lines (HeLa, RAW and dTHP-1) was investigated using flow cytometry. The cells were incubated with either spherical or cylindrical capsules at a capsule-to-cell ratio of 100 : 1 for 24 h at 37 °C. Our data show that cylindrical capsules exhibit decreased association with HeLa cells (54%) compared with their spherical counterparts (81%) after 24 h incubation (Fig. 2A). This is consistent with our previous study on shape dependent cellular association of polymer capsules in HeLa cells, where a lower internalisation was observed for higher aspect ratio (AR) capsules.[18] This is likely attributed to the larger average radius or surface area the cells may endure during endocytosis.[29] However, in murine macrophage RAW cells, the cylindrical capsules appeared to have an enhanced association (97%) after 24 h incubation compared with spherical capsules (86%) (Fig. 2B), which indicates that bigger capsules were phagocytized more readily than smaller ones by RAW cells. Meanwhile, for dTHP-1 cells, cellular association appeared independent of PMA_{SH} capsule shape, as different shapes did not result in a significant difference in cellular association after 24 h (Fig. 2C). Spherical capsules (D = 390 nm) were associated with RAW and dTHP-1 cells to a similar degree. This is consistent with a recent report where fluoromica nanoparticles with different diameters (D = 250, 600 and 1000 nm) showed comparable uptake in RAW and dTHP-1 cells.[30] However, cylindrical capsules associated with RAW cells to a greater degree than dTHP-1 cells for all time points. This was particularly obvious in the first 2 h of incubation, when the cellular association of cylindrical PMA_{SH} capsules with RAW cells already reached 75%. In contrast, it took approximately 6 h for the same capsules to reach the same level of association with dTHP-1 cells. This suggests that the RAW cells exhibit a stronger affinity to associate with the dimensionally larger cylindrical PMA_{SH} capsules compared to dTHP-1 cells. Altogether, these data demonstrate that the effect of PMA_{SH} capsule shape on cellular association is cell line-dependent. Moreover, spherical capsules experienced similar cellular association in all three cell lines (HeLa, RAW and dTHP-1 cells after 24 h incubation), while the cellular association differed in all cases for cylindrical PMA_{SH} capsules (Fig. 2D).

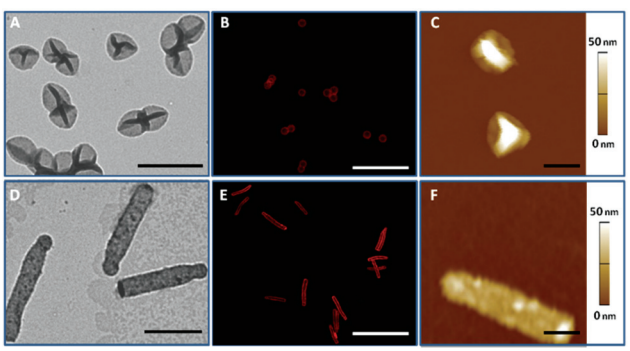

Fig. 1 Representative TEM (A, D), SIM (B, E), and AFM (C, F) images of PMA_{SH} capsules: (A, B, C) spherical capsules and (D, E, F) cylindrical capsules. Scale bars in A and D are 1 μm, in B and E are 4 μm, and in C and F are 0.5 μm.

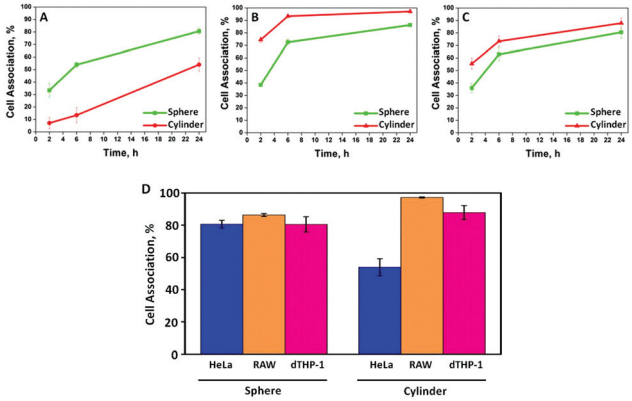

Fig. 2 Cellular association kinetics of spherical (green) and cylindrical (red) PMA_{SH} capsules in: (A) HeLa, (B) RAW, and (C) dTHP-1 cells after 2 h, 6 h and 24 h incubation at 37 °C, 5% CO_2. (D) Comparison of the three cell lines and their individual levels of association with spherical (left) and cylindrical (right) PMA_{SH} capsules after 24 h incubation. The data are represented as mean ± standard error from three independent experiments, and at least 10 000 cells analysed in each experiment using flow cytometry.

3.3 Intracellular deformation of spherical PMA_{SH} capsules

Next, we investigated the intracellular deformation of PMA_{SH} capsules in different cell lines. PMA_{SH} capsules were incubated with HeLa, RAW or dTHP-1 cells at 37 °C for 24 h. Subsequently, the cells were fixed, and the cell membranes were stained with AF488 WGA followed by super high resolution imaging using SIM. After incubation with cells, the spherical PMA_{SH} capsules were found to be both internalised and surface bound for all three different types of cells (Fig. 3). In the case of HeLa cells, the internalised capsules appeared to be highly compressed, morphologically changing from the original hollow spheres to "dense particle" structures, and showing increased fluorescence intensity (Fig. 3A). In contrast, the internalised capsules were less deformed in RAW cells, appearing as hollow crescent-like and ellipsoid-like structures (Fig. 3B). In dTHP-1 cells, almost all internalised capsules maintained their hollow spherical structures (Fig. 3C). This is consistent with previous reports that polyelectrolyte multilayer capsules gradually buckle and deform during internalisation into human breast cell lines, indicating that only polymer capsules with reinforced stiffness were able to withstand cell-generated mechanical forces during the uptake process.[8] Notably, the deformation of capsules outside but already attached to the cell membrane was also observed with HeLa cells (Fig. 3A, inset). This suggests that deformation starts to occur at the engagement between capsules and the cell membrane during the early stages of internalisation. The intracellular deformation of capsules was quantified using a deformation percentage defined as the number of deformed capsules divided by the number of total (deformed and non-deformed) capsules after internalisation. Hence, intracellular capsule deformation levels of 96%, 56% and 29% were observed for HeLa, RAW and dTHP-1 cells, respectively (analysing at least 300 internalised capsules). Due to the differing deformation exhibited by identical spherical capsules, we propose that HeLa cells generate higher mechanical forces, followed by RAW cells and dTHP-1 cells during their internalisation processes. Our previous study demonstrated that at pH below the pK_a of PMA (pH = 6.5), the stiffness of PMA_{SH} films increased dramatically due to protonation of the carboxyl group on the polymer backbone.[31] Thus, pH differences that exist between the extracellular and intracellular environment may also contribute to the deformation of PMA_{SH} capsules after internalisation. We examined the intracellular localisation of the spherical PMA_{SH} capsules in different cells. The internalised capsules appeared to be mainly located in the late endosomes and lysosomes (pH = 4.5–5.5) in all cell types (Fig. S3†). Since the capsules had the same intracellular fate, it appears that pH is an unlikely factor in the intracellular deformation of capsules in different cells. Next, we investigated if the redox-triggered (bio)degradability of disulfide crosslinked PMA_{SH} capsules influenced the intracellular deformation of PMA_{SH} capsules. Disulfide crosslinked PMA_{SH} capsules degrade in the presence of GSH, an abundant reductive agent found inside cells, including endosomes and lysosomes.[32] We compared the deformation of non-degradable and degradable PMA_{SH} capsules after internalisation by cells. Non-degradable PMA_{SH} capsules were prepared using $BM(PEG)_2$, a linker that induces a noncleavable covalent bond when reacted with thiol groups (as shown in Fig. S4†). It was observed that non-degradable spherical PMA_{SH} capsules also deformed (92%) in HeLa cells after 24 h incubation, with levels comparable to that of degradable PMA_{SH} capsules (Fig. S5A†). Meanwhile, we observed that 59% and 21% of non-degradable capsules deformed in RAW and dTHP-1 cells, respectively (Fig. S5B and C†). Despite the slight differences (4% in HeLa, 3% in RAW and 8% in dTHP-1 cells) in the percentage of deformation of degradable and non-degradable PMA_{SH} capsules in all cell lines studied, these differences are not significant enough to suggest that the deformation of PMA_{SH} capsules during internalisation is dominated by destabilisation of the PMA_{SH} polymer layers. Rather, the intracellular deformation of the PMA_{SH} capsules suggests that the capsules are subjected to differing magnitudes of mechanical force during internalisation by HeLa, RAW and dTHP-1 cells, which is consistent with the literature, which suggests that cell mechanical forces can differ significantly for different cells types.[33] Although techniques to quantify mechanical stress in living cells during dynamic uptake processes are not yet available, the intracellular forces exerted by a cell upon internalisation of particulates is believed to be one of the key parameters to successful delivery.[34]

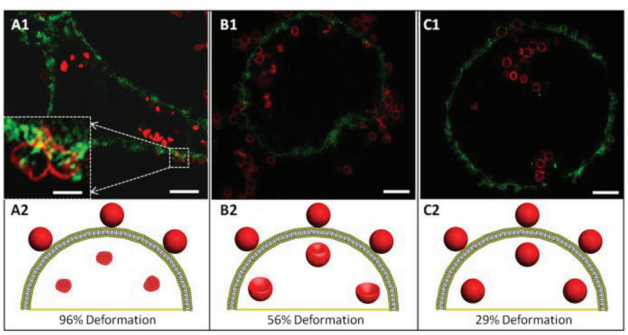

Fig. 3 SIM images of AF633-labelled spherical PMA_{SH} capsules in HeLa (A), RAW (B), and dTHP-1 (C) cells after 24 h incubation at 37 °C, 5% CO_2. The inset of A1 represents the magnification of the frame area in A1. Images of A1–C1 represent a single *z*-plane image of cells. Cell membranes were stained with AF488 WGA. Scale bars in A1–C1 are 2.5 μm and 0.5 μm in the inset of A1. A2–C2 schematically illustrate the various deformations of capsules inside cells.

3.4 Intracellular deformation of cylindrical PMA_{SH} capsules

To investigate the possible effect of shape on capsule deformation, we treated the cells with cylindrical PMA_{SH} capsules for 24 h to allow significant internalisation (see Fig. 4). It was observed that the cylindrical PMA_{SH} capsules were compressed and lost their cylindrical shapes inside HeLa cells (Fig. 4A and D), whereas they were partially deformed after internalisation by RAW cells (Fig. 4B and E), and largely retained their dimensions and hollow morphology within dTHP-1 cells (Fig. 4C and F). The intracellular deformation of these cylindrical capsules

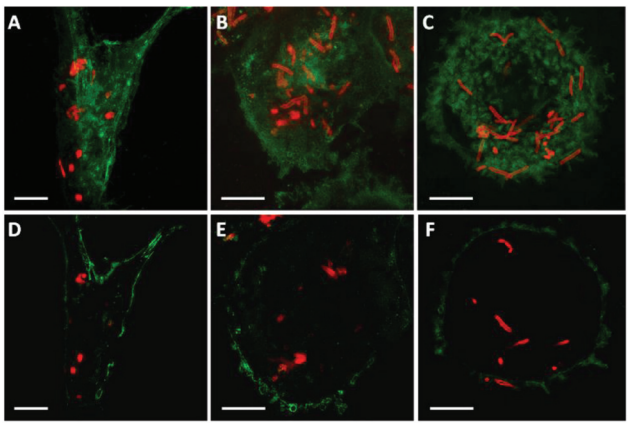

Fig. 4 SIM images of AF633-labelled cylindrical PMA_{SH} capsules in HeLa (A, D), RAW (B, E), and dTHP-1 (C, F) cells after 24 h incubation at 37 °C, 5% CO_2. Images A, B, and C are presented at the maximum intensity projection. Images D, E, and F represent single *z*-plane images A, B, and C, respectively. Cell membranes were stained with AF488 WGA. Scale bars are 5 μm.

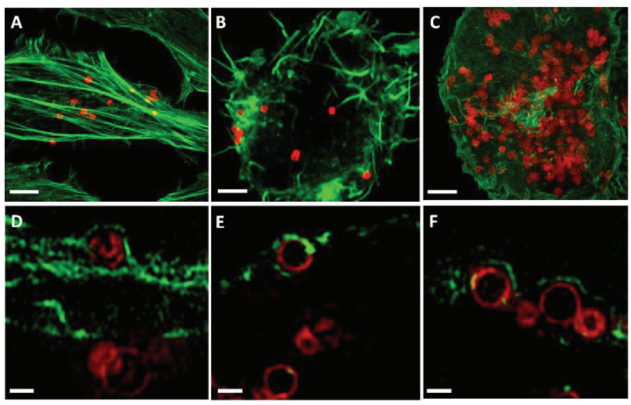

Fig. 5 SIM images of AF633-labelled PMA_{SH} capsules with spherical shapes in HeLa (A, D), RAW (B, E) and dTHP-1 (C, F). Cell actin was stained with AF488 phalloidin. Images A, B, and C present images at the maximum intensity projection and images D, E, and F represent a single *z*-plane image of cells. The capsules were incubated with all cell types for 24 h at 37 °C, 5% CO_2. Scale bars: A–C, 2.5 μm; D–F, 0.5 μm.

is in line with that of spherical capsules, where we found that HeLa cells subjected capsules to the highest mechanical forces during their uptake process, followed by RAW cells, and then dTHP-1 cells.

3.5 Actin-mediated intracellular deformation of PMA_{SH} capsules

Previous studies have speculated that polymer capsules are engulfed into cells through the formation of large cytoplasmic protrusions regulated by actin movement.[13,35] Actin filaments are particularly abundant beneath the plasma membrane, where they form a network that provides mechanical support for the cell and facilitates the movement that leads to the engulfment of external particles.[36] In addition, actin filaments play a role in the process of endocytosis, which may contribute to cellular osmotic pressure.[35] Therefore, to elucidate the influence of cell-generated mechanical forces on intracellular deformation, the role of actin was investigated. Spherical PMA_{SH} capsules were incubated with all cell types for 24 h. Subsequently, the cells were fixed and the actin was fluorescently stained with AF488 phalloidin to allow imaging using SIM. Long and thick horizontal actin filaments were observed in HeLa cells (Fig. 5A). Short strands of thick actin filaments were observed in RAW cells (Fig. 5B) and a meshwork pattern of thin actin filaments was observed in dTHP-1 cells (Fig. 5C). Different actin patterns arise from the assembly of actin filaments, which is governed by a variety of actin-binding proteins that crosslink actin filaments in distinct structures in different cell lines.[37] By staining the actin filaments, protrusions that surround the PMA_{SH} capsules were observed for all three types of cells (Fig. 5D–F). Importantly, the actin filaments surrounding capsules showed different morphologies with each cell line. In the case of HeLa cells, the capsules are largely compressed after being surrounded by the actin filament protrusions (Fig. 5D). However, the actin appears to have little effect on the morphology of the capsules in RAW and dTHP-1 cells (Fig. 5E and F). These observations indicate that the PMA_{SH} capsules undergo a greater deformation as a result of the higher mechanical forces enforced by the denser actin filaments of HeLa cells compared with RAW and dTHP-1 cells. This is in agreement with previous studies that the actin filament movement requires mechanical forces in the range of tens of piconewtons to hundreds of nanonewtons that vary among different cell types.[38] We believe this is likely due to the different endocytic pathways between epithelial cells (HeLa) and phagocytic cells (RAW and dTHP-1), which regulate cells with differential abilities to internalise polymer capsules, resulting in the different deformation of the capsules.

4 Conclusions

We investigated the intracellular deformation of spherical and cylindrical polymer capsules in HeLa, RAW and dTHP-1 cells using super high resolution microscopy. Our data showed a similar association of spherical PMA_{SH} capsules between the three cell lines, but revealed that the intracellular deformation of capsules was cell line-dependent, which may arise from the different degrees of mechanical forces generated by cells during the internalisation process. Spherical capsule deformation was highest in HeLa cells (96%), followed by RAW (56%), then dTHP-1 cells (29%). A similar trend of cell line-dependent deformation was also observed with cylindrical capsules, despite the higher association of the cylindrical capsules to the RAW/dTHP-1 cells compared with HeLa cells. The detailed measurement of mechanical forces of cells during their dynamic uptake processes warrants further investigation. However, our findings reveal that intracellular processing based on capsule deformation is cell line-dependent given the

identical physicochemical properties of the capsules studied. The use of SIM to image intracellular deformation provides a means to explore the interactions between polymer capsules and biological systems, which in turn can guide the design of polymer capsules for effective drug delivery, as well as drive fundamental understandings in cell mechanobiology.

Acknowledgements

This research was conducted and funded by the Australian Research Council (ARC) Centre of Excellence in Convergent Bio-Nano Science and Technology (project number CE140100036). This work was also supported by the ARC under the Australian Laureate Fellowship (F. C., FL120100030), the Discovery Early Career Researcher Award (Y. Y., DE130100488), and the Super Science Fellowship (F. C., FS110200025) schemes. We thank Dr Christina Cortez-Jugo (the University of Melbourne) and Benjamin Hibbs (the Materials Characterisation and Fabrication Platform) for helpful discussions. M. M. thanks the University of Melbourne for support through a McKenzie Fellowship. This work was performed in part at the Materials Characterisation and Fabrication Platform (MCFP) at the University of Melbourne and the Victorian Node of the Australian National Fabrication Facility (ANFF).

Notes and references

1 J. Cui, M. P. van Koeverden, M. Müllner, K. Kempe and F. Caruso, *Adv. Colloid Interface Sci.*, 2014, **207**, 14–31.
2 J. Gaitzsch, X. Huang and B. Voit, *Chem. Rev.*, 2016, **116**, 1053–1093.
3 P. T. Hammond, *Nanomedicine*, 2012, **7**, 619–622.
4 C. E. Mora-Huertas, H. Fessi and A. Elaissari, *Int. J. Pharm.*, 2010, **385**, 113–142.
5 Y. Yan, M. Björnmalm and F. Caruso, *Chem. Mater.*, 2014, **26**, 452–460.
6 P. Watson, A. T. Jones and D. J. Stephens, *Adv. Drug Delivery Rev.*, 2005, **57**, 43–61.
7 S. De Koker, L. J. De Cock, P. Rivera-Gil, W. J. Parak, R. Auzély Velty, C. Vervaet, J. P. Remon, J. Grooten and B. G. De Geest, *Adv. Drug Delivery. Rev.*, 2011, **63**, 748–761.
8 A. Muñoz Javier, O. Kreft, M. Semmling, S. Kempter, A. G. Skirtach, O. T. Bruns, P. del Pino, M. F. Bedard, J. Rädler, J. Käs, C. Plank, G. B. Sukhorukov and W. J. Parak, *Adv. Mater.*, 2008, **20**, 4281–4287.
9 M. F. Bédard, A. Munoz-Javier, R. Mueller, P. del Pino, A. Fery, W. J. Parak, A. G. Skirtach and G. B. Sukhorukov, *Soft Matter*, 2009, **5**, 148–155.
10 B. G. De Geest, R. E. Vandenbroucke, A. M. Guenther, G. B. Sukhorukov, W. E. Hennink, N. N. Sanders, J. Demeester and S. C. De Smedt, *Adv. Mater.*, 2006, **18**, 1005–1009.
11 G. B. Sukhorukov, A. L. Rogach, B. Zebli, T. Liedl, A. G. Skirtach, K. Kohler, A. A. Antipov, N. Gaponik, A. S. Susha, M. Winterhalter and W. J. Parak, *Small*, 2005, **1**, 194–200.
12 M. Delcea, S. Schmidt, R. Palankar, P. A. Fernandes, A. Fery, H. Möhwald and A. G. Skirtach, *Small*, 2010, **6**, 2858–2862.
13 R. Palankar, B.-E. Pinchasik, S. Schmidt, B. G. De Geest, A. Fery, H. Möhwald, A. G. Skirtach and M. Delcea, *J. Mater. Chem.*, 2013, **1**, 1175–1181.
14 Y. Yan, A. P. R. Johnston, S. J. Dodds, M. M. J. Kamphuis, C. Ferguson, R. G. Parton, E. C. Nice, J. K. Heath and F. Caruso, *ACS Nano*, 2010, **4**, 2928–2936.
15 P. Rivera-Gil, S. De Koker, B. G. De Geest and W. J. Parak, *Nano Lett.*, 2009, **9**, 4398–4402.
16 A. Muñoz Javier, O. Kreft, M. Semmling, S. Kempter, A. G. Skirtach, O. T. Bruns, P. del Pino, M. F. Bedard, J. Rädler, J. Käs, C. Plank, G. B. Sukhorukov and W. J. Parak, *Adv. Mater.*, 2008, **20**, 4281–4287.
17 B. Huang, M. Bates and X. Zhuang, *Annu. Rev. Biochem.*, 2009, **78**, 993–1016.
18 O. Shimoni, Y. Yan, Y. Wang and F. Caruso, *ACS Nano*, 2013, **7**, 522–530.
19 K. T. Gause, Y. Yan, J. Cui, N. M. O'Brien-Simpson, J. C. Lenzo, E. C. Reynolds and F. Caruso, *ACS Nano*, 2015, **9**, 2433–2444.
20 Y. Yan, K. T. Gause, M. M. J. Kamphuis, C.-S. Ang, N. M. O'Brien-Simpson, J. C. Lenzo, E. C. Reynolds, E. C. Nice and F. Caruso, *ACS Nano*, 2013, **7**, 10960–10970.
21 S. De Koker, J. Cui, N. Vanparijs, L. Albertazzi, J. Grooten, F. Caruso and B. G. De Geest, *Angew. Chem., Int. Ed.*, 2016, **55**, 1334–1339.
22 D. van der Zwaag, N. Vanparijs, S. Wijnands, R. De Rycke, B. G. De Geest and L. Albertazzi, *ACS Appl. Mater. Interfaces*, 2016, **8**, 6391–6399.
23 J. Cui, B. Hibbs, S. T. Gunawan, J. A. Braunger, X. Chen, J. J. Richardson, E. Hanssen and F. Caruso, *Langmuir*, 2016, **32**, 3532–3540.
24 M. G. L. Gustafsson, *Proc. Natl. Acad. Sci. U. S. A.*, 2005, **102**, 13081–13086.
25 A. Jost and R. Heintzmann, *Annu. Rev. Mater. Res.*, 2013, **43**, 261–282.
26 A. N. Zelikin, Q. Li and F. Caruso, *Chem. Mater.*, 2008, **20**, 2655–2661.
27 A. Kuijk, A. van Blaaderen and A. Imhof, *J. Am. Chem. Soc.*, 2011, **133**, 2346–2349.
28 X. Chen, Y. Yan, M. Müllner, Y. Ping, J. Cui, K. Kempe, C. Cortez-Jugo and F. Caruso, *Biomacromolecules*, 2016, **17**, 1205–1212.
29 J.-W. Yoo, N. Doshi and S. Mitragotri, *Macromol. Rapid Commun.*, 2010, **31**, 142–148.
30 N. Tee, Y. Zhu, G. M. Mortimer, D. J. Martin and R. F. Minchin, *Int. J. Nanomed.*, 2015, **10**, 2363–2375.
31 J. P. Best, M. P. Neubauer, S. Javed, H. H. Dam, A. Fery and F. Caruso, *Langmuir*, 2013, **29**, 9814–9823.

32 F. Meng, Z. Zhong and J. Feijen, *Biomacromolecules*, 2009, **10**, 197–209.
33 T. G. Kuznetsova, M. N. Starodubtseva, N. I. Yegorenkov, S. A. Chizhik and R. I. Zhdanov, *Micron*, 2007, **38**, 824–833.
34 R. Hartmann, M. Weidenbach, M. Neubauer, A. Fery and W. J. Parak, *Angew. Chem., Int. Ed.*, 2015, **54**, 1365–1368.
35 O. L. Mooren, B. J. Galletta and J. A. Cooper, *Annu. Rev. Biochem.*, 2012, **81**, 661–686.
36 G. M. Cooper, *Structure and Organization of Actin Filaments*, Sinauer Associates, Sunderland, MA, 2nd edn, 2000.
37 C. G. dos Remedios, D. Chhabra, M. Kekic, I. V. Dedova, M. Tsubakihara, D. A. Berry and N. J. Nosworthy, *Physiol. Rev.*, 2003, **83**, 433–473.
38 R. Ananthakrishnan and A. Ehrlicher, *Int. J. Biol. Sci.*, 2007, **3**, 303–317.